Mechanical behaviour of corroded strands under chloride attack: A new constitutive law

Mechanical behaviour of corroded strands under chloride attack: A new constitutive law

Lorenzo Franceschini [a], Francesca Vecchi [a], Francesco Tondolo [b], Beatrice Belletti [a,*], Javier Sánchez Montero [c]

[a] Department of Engineering and Architecture, University of Parma, Parco Area delle Scienze 181/A, 43124 Parma, Italy
[b] Department of Structural, Geotechnical and Building Engineering, Politecnico di Torino, Corso Duca degli Abruzzi 24, 10129 Turin, Italy
[c] Institute Eduardo Torroja of Construction Sciences (IETcc-CSIC), Serrano Galvache, Madrid, Spain

Keywords:
Pitting corrosion
Constitutive law
Prestressing strands
Tensile tests
Digital Image Correlation
3D scan

A B S T R A C T

The paper presents an experimental and analytical study on the tensile behaviour of naturally corroded prestressing strands. A total of twenty-four strands were extracted from full-scale beams which were exposed during 10 years to chlorides from sea water. Firstly, a database has been created on the dependency of the maximum pit depth on the strand mass loss or on the section loss of the most corroded wire. Secondly, the morphology of corrosion pits and the maximum cross-sectional loss of each external wire have been measured. Finally, based on conducted tensile tests, a new constitutive law (CPS-model) is proposed to predict the mechanical behaviour of prestressing strands induced by pitting corrosion.

1. Introduction

In the last twenty years, the attention of the scientific community on the impact of corrosion deterioration process in the maintenance of existing structures and infrastructures - such as bridges [1,2] - has seen an exponential increasing interest worldwide. In order to limit economic and human losses [3,4] the scientific and the technical communities, the public and private authorities, and the administrations are facing the issues related to malfunctioning or failures of corroded reinforced concrete (RC) and prestressed concrete (PC) members. RC and PC structures can be subjected to corrosion, either by carbonation of the concrete or by the action of chlorides. The present paper focuses on PC members exposed to marine environments, like costal area and/or components exposed to de-icing salts, which are strongly affected by chloride-induced corrosion deterioration.

The main effects of corrosion in RC and PC members are the cracking or spalling of concrete cover - caused by formation of rust products -, the reduction of the mechanical properties of the steel, the section and mass loss, and the bond strength [5,6]. In RC and PC structures, the corrosion of steel leads to the decrease of stiffness, ductility and load carrying capacity of members. Moreover, in PC members heavily corroded, the relevant reduction of the ductility and the cross-sectional area of wires may cause the fracture of one or more strands, leading to brittle failures that occur without visual warning signs [1,7].

The morphology of the damage in prestressing strands, induced by pitting corrosion, has not been widely investigated such as in reinforcing rebars. In particular, Val and Melchers [8,9] proposed an hemispherical pit configuration for the evaluation of the cross-sectional area of the most corroded wire. According to observations from specimens belonging to existing bridges, Jeon et al., [10] introduced three different pit types for the description of the damage morphology induced by corrosion in strands. Additionally, limited literature is available on reliable values of the pitting factor, which represents the ratio between the maximum and the average pit depth in strands, [11,12]. Vecchi et al., [12] proposed a pitting factor equal to 1.5 for naturally corroded strands.

The paper presents a database that collects the measurements available in literature including the maximum pit depth, the ultimate strength, and the ultimate strain of corroded prestressing strands as a function of the mass loss of the prestressing strand or the cross-sectional loss of the prestressing strand. In this context, the additional data presented in this paper can be useful to perform probabilistic estimations of the mechanical properties of corroded strands.

The state of the art, related to the estimation of the tensile response

of corroded prestressing strands, is limited and faces the topic according to two different main approaches: the first approach evaluates the corroded strand as a rebar, while the second approach estimates the overall behaviour of the corroded strand by adding the single contributions of each wire. According to the first approach, a simplified elastic-hardening model was proposed by Zona et al., [13], by Wang et al., [14] and Lu et al., [15]. The model introduced an area damage factor for the estimation of the reduced mechanical properties required to obtain the stress–strain relationship. According to the second approach, an equivalent spring model was proposed by Jeon et al., [10], while Zhang et al., [7] established a stochastic stress–strain relationship for corroded prestressing wires based on random generation of cross-sectional areas. However, there is a lack of data in literature comparing natural corrosion pitting characterization with mechanical test results, such as strength and ductility of prestressing strands. For example, the model proposed by Jeon et al., [10] is based on the response of wires determined from non-linear finite element analyses.

The present work proposes a new reliable constitutive model, named CPS-model, for the prediction of the mechanical behaviour of corroded prestressing strands based on pit morphology, maximum pit depth, cross-sectional loss, and mass-loss variation. In the framework of the second approach, the proposed stress–strain relationship for corroded prestressing strands represents the main novelty of this paper because it is based on experimental data on pits morphology and results of tensile tests carried out on naturally corroded specimens extracted from full-scale beams.

Firstly, in section 2, the twenty-four prestressing strand samples - retrieved from previously tested PC beams - are described. In section 3, the data on the pits morphology - accurately analysed by means of a 3D laser scanner - and on the mass-loss - measured according to ASTM G1-03 Standard [16] - are illustrated. The data is post-processed with the GOM Inspect software to measure the average and maximum pit depth for each wire and therefore the section loss for each wire. The maximum pit depth of each wire has been classified according to the pit type morphologies defined by Jeon et al., [10]. Then, a new correlation between maximum pit depth and cross-sectional loss of the most corroded wire is proposed. Secondly, in section 4, the mechanical results of the tensile tests carried out on twenty-four samples in the Laboratory MastrLab of Politecnico di Torino are shown. Thereafter, the stress–-strain relationships are obtained by adopting the Digital Image Correlation (DIC) methodology. Finally, in section 5 the CPS-model is presented. The accuracy and the reliability of CPS-model is validated by comparing the predicted tensile behaviour with the results of the experimental test presented in this paper and with the results obtained by adopting the model proposed by Jeon et al., [10]. Furthermore, regression analyses have been carried out to estimate the dependency of the ultimate strength and the ultimate strain on the cross-sectional loss of the most corroded wire. The regression analysis enables the CPS-model to depend on input data that can be collected during in-situ inspections, such as the maximum pit depth. In the present study in-situ measurements' techniques are not treated.

The impact of the paper in the engineering practice is the improvement in the prediction of the tensile behaviour of corroded prestressing strands, which allows a more reliable assessment of the capacity of corroded PC members and more accurate estimation of the residual life of existing PC structures.

2. Details of prestressing strand samples

A total of twenty-four prestressing strands were retrieved from 10 years old natural corroded PC beams. The analysed PC beams came from a refrigeration tower of a thermal power-plant where for 10 years, they were exposed to wet and dry cycles carried out by using sea water. The PC beams were reinforced with two seven-wire strands with an equivalent diameter equal to 12.9 mm. The six external wires and the core wire had a radius equal to 2.13 mm (r_{outer}) and 2.19 mm (r_{inner}), respectively. The un-corroded cross-sectional area of the strand was about 100 mm^2, while the area of inner and outer wires was equal to 15 mm^2 and 14.22 mm^2, respectively. The material used is cold drawn steel, which is a eutectoid steel with a pearlitic microstructure. For more information please refer to [17–19]. Since the collected samples came from different beams at different locations, the level of corrosion varied from sample to sample; furthermore, un-corroded samples were collected to obtain reference data of geometrical and mechanical properties of strands without degradation induced by corrosion. In particular, since the beam ends were not properly protected and no concrete cover was provided to avoid the chloride-induced corrosion process, the most corroded prestressing strands were generally found out in correspondence of these external regions. On the other hand, when relevant cracks - induced by corrosion deterioration - were not observed along the length of the PC beams, the prestressing strands placed in proximity to the mid-span of the PC beams were not influenced by the corrosion process. Thus, the un-corroded samples were retrieved from these unaffected regions after a detailed visual inspection. More information about the tests set-up and PC beams characteristics can be found in [20–21]. Thereafter, the collected samples were subdivided into two main groups characterised by two different lengths. The first group consisted of twelve prestressing strands 450 mm long, whereas the second group consisted of twelve prestressing strands 700 mm long. Each sample has been identified with a code (see Table 1). The code consists of a series of letters and numbers, where PB stands for prestressed beams followed by a number from 9 to 14 indicating the name of the reference beam; then, the letter L or R, which stands for left or right, respectively, is added to specify the cross-sectional position of the retrieved sample; finally, the position of sample along the beam span is identified by numbers in brackets that represent the initial and final abscissa.

3. Experimental data on pits morphology and section loss

3.1. Measurements of damage induced by corrosion

Fig. 1 schematically shows the phases of the experimental tests carried out on the corroded samples.

Before tensile tests, the mass loss, η_s, of each collected sample has been firstly evaluated according to the procedure described in ASTM G1-03 Standard [16]. Since four out of twenty-four samples - named PB9-R (428–473), PB11-L(5–75), PB12-R(358–403), and PB14-L(455–500) - were un-corroded, they have been assumed as reference specimens in the following calculations. Moreover, since experimental recording problems have been experienced during the testing of PB10-R(32–102) and PB14-R(77–122) samples, their experimental data have been neglected. Therefore, the dependency of the tensile behaviour on the morphology of the damage induced by pitting corrosion has been deeply investigated for a total of 18 samples. Table 1 reports the maximum pit depth, P_{max}, the average pit depth, P_{av}, the maximum cross-sectional loss, μ_{loss}, and the pit type morphology of the most corroded wire measured in each sample.

The mass loss, η_s, of each corroded sample has been calculated as given in Eq. (1) and has been reported in Table 1:

$$\eta_s = \frac{m_0 - m_{cor}}{m_0} \tag{1}$$

where m_0 is the un-corroded mass of the sample - equal to 359.73 g and 559.59 g for the samples of 450 mm long and 700 mm long, respectively -, while m_{cor} is the residual mass of sample, measured according to ASTM G1-03 Standard.

Secondly, the pits depth and the pits morphology in each wire - along the length of samples -, have been accurately measured. In correspondence of the maximum pit depth detected, the residual cross-section area has been measured. The ATOS Compact structured light 3D scanner,

Table 1
Samples main features: L_i is the sample length, η_s is the mass loss of the corroded sample, P_{max} is the maximum pit depth, P_{av} is the average pit depth, μ_{loss} is the cross-sectional loss of the most corroded wire, and Pit Type is the morphology configuration of the most corroded wire evaluated according to [10].

Strand				Most corroded wire			
Sample ID°	Beam	L_i[mm]	η_s[%]	P_{max}[mm]	P_{av}[mm]	μ_{loss}[%]	Pit Type
PB9-L(12–82)	PB4P9	700	17.3	1.711	1.14	37.58	3
PB9-L(426–496)	PB4P9	700	2.8	0.424	0.28	3.67	1
PB9-R(15–60)	PB4P9	450	21.5	2.784	1.85	69.20	3
PB9-R(428–473)	PB4P9	450	–	–	–	–	–
PB10-L(138–208)	PB3P10	700	2.4	0.590	0.39	8.39	3
PB10-L(445–515)	PB3P10	700	6.3	2.570	1.71	59.61	3
PB10-R(32–102)	PB3P10	700	2.2	Negl.	Negl.	Negl.	Negl.
PB10-R(287–332)	PB3P10	450	8.0	2.880	1.91	59.60	1
PB11-L(5–75)	PB3P11	700	–	–	–	–	–
PB11-L(196–266)	PB3P11	700	2.9	1.402	0.93	28.66	3
PB11-R(6–51)	PB3P11	450	2.0	0.976	0.65	17.51	3
PB11-R(273–318)	PB3P11	450	4.8	1.260	0.83	23.48	3
PB12-L(12–82)	PB3P12	700	14.2	1.630	1.08	36.85	2
PB12-L(124–169)	PB3P12	450	4.3	1.227	0.82	23.96	3
PB12-R(100–170)	PB3P12	700	5.3	1.040	0.69	15.20	3
PB12-R(358–403)	PB3P12	450	–	–	–	–	–
PB13-L(1–46)	PB4P13	450	7.6	1.460	0.97	22.85	1
PB13-L(108–178)	PB4P13	700	4.3	1.760	1.17	34.38	3
PB13-R(0–70)	PB4P13	700	11.4	1.570	1.04	27.02	2
PB13-R(70–115)	PB4P13	450	4.6	1.090	0.72	20.23	3
PB14-L(10–55)	PB4P14	450	14.7	2.237	1.49	53.06	3
PB14-L(455–500)	PB4P14	450	–	–	–	–	–
PB14-R(2–72)	PB4P14	700	11.6	1.227	0.82	23.69	3
PB14-R(77–122)	PB4P14	450	3.8	Negl.	Negl.	Negl.	Negl.

characterised by a stereoscopic vision enabled by means of two 2-megapixel cameras, has been used to detect the actual pits morphology induced by corrosion deterioration. Afterwards, once the scanning phase has been completed and the cloud of points scattered in space has been recorded, the virtual model of the geometry of the sample has been obtained by converting the data points into tessellated surface with the use of triangles.

Thirdly, by importing the virtual model in .SLT format into GOM Inspect software, the comparison between the un-corroded reference sample and the corroded ones has been carried out by means of a superposition procedure. Based on software outcomes, the maximum pit depth, P_{max}, the number of pits, the distribution of pits along the length of the sample, the area of pits, A_p, the average area of pits, A_{av}, and the minimum cross-sectional area, A_{min}, have been measured. Generally, the core wire has been assumed as un-corroded. It is worth noting that the accuracy of the obtained results - by using GOM Inspect software - has been certified by the German PTB Institute and the American NIST Institute.

Then, the maximum pit of each corroded sample has been classified by means of the comparison between the area loss, measured from GOM Inspect software and AutoCAD outcomes, and the area loss, A_p, calculated according to formulations, proposed by Jeon et al., [10], for the three pit type morphologies, as given from Eq. (2) to Eq. (4):

$$A_{p,1} = 2r_{outer}^2(\vartheta_1 - 2sin\vartheta_1 cos\vartheta_1) \qquad \vartheta_1 = arccos\left(1 - \frac{P_{max}}{2r_{outer}}\right) \tag{2}$$

$$A_{p,2} = r_{outer}^2(2\vartheta_2 - \pi - 2sin\vartheta_2 cos\vartheta_2) \qquad \vartheta_2 = arccos\left(-\frac{P_{max}}{2r_{outer}}\right) \tag{3}$$

$$A_{p,3} = r_{outer}^2(\vartheta_3 - sin\vartheta_3 cos\vartheta_3) \qquad \vartheta_3 = arccos\left(1 - \frac{P_{max}}{r_{outer}}\right) \tag{4}$$

where θ_1, θ_2, θ_3 are the corrosion angles related to the different pit shapes [10] and r_{outer} is the radius of the external wire.

Thereafter, the average pit depth, P_{av}, - reported in Table 1 - has been estimated as a function of the maximum pit depth, P_{max}, according to the formulation proposed by Vecchi et al., [12], as given in Eq. (5):

$$P_{av} = 0.6638 \cdot P_{max} \tag{5}$$

Finally, the maximum cross-sectional loss, μ_{loss}, of each wire has been calculated according to Eq. (6), in correspondence of the section where the maximum pit depth, P_{max}, was measured:

$$\mu_{loss} = \frac{A_p}{A_{outwire,0}} \tag{6}$$

where $A_{outwire,0}$ is the un-corroded cross-sectional area of the external wire.

In general, once the cross-sectional loss of each wire has been estimated, the cross-sectional loss of the corroded strand - at the same section - has been given by the sum of the cross-sectional losses evaluated for the seven wires. In this regard, according to the scientific literature [10,14], the mass loss and the maximum cross-sectional loss are generally recognized as the two main parameters for the evaluation of the corrosion deterioration of prestressing strands. However, since the mass loss mainly reflects the average corrosion of a strand along its entire length, this latter parameter should be used only for the estimation of the mechanical behaviour of corroded strands subjected to uniform corrosion and results improperly used for strands subjected to localised corrosion (pitting). In this context, the maximum cross-sectional loss, which better reproduces the effects associated to local corrosion, should be used in case of pitting corrosion for the estimation of the mechanical behaviour of corroded prestressing strands.

In addition, as confirmed by Jeon et al., [10], up to now several researches have been carried out to find the pit type morphology that allows a simplified calculation of the cross-sectional loss as a function of the maximum pit depth, P_{max}, [8,15]. However, this simplified assumption enables to evaluate the damage pattern related to similar pits type morphologies. Conversely, any damage pattern can be evaluated by considering the three pit type morphologies illustrated in Fig. 1. Moreover, the *in-situ* activities for detection of the damage induced by localised corrosion can be potentially facilitated by the visual comparison with the three pit type morphologies illustrated in Fig. 1. Therefore,

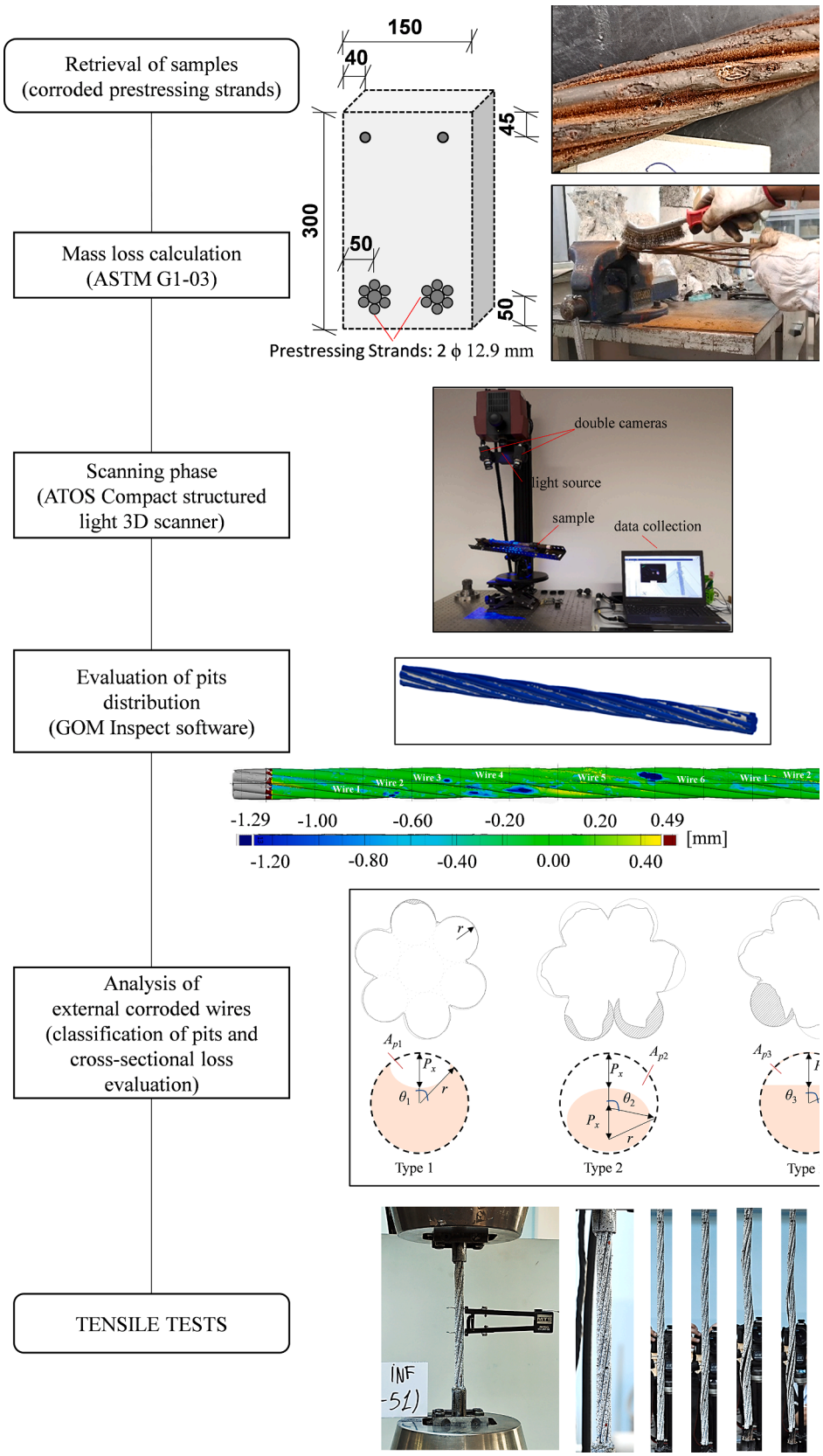

Fig. 1. Flow-chart of the preliminary procedure concerning corroded prestressing strand samples.

in this paper the maximum cross-sectional loss of wires, calculated according to Eqs.(2)-(4) depending on the three pit type morphologies, is assumed as the main parameter for the proposed CPS-model.

3.2. The database used to correlate the maximum pit depth with the section-loss of the most corroded wire

A database of tests on strands with natural chloride corrosion is created. Fig. 2 shows a combination between the results of the present work and the outcomes reported in Vecchi et al., [12], which is indicated by red markers and the outcomes presented by Wang et al., [14], which is indicated with grey markers. In particular, the relationship between the maximum pit depth, P_{max}, measured in each corroded sample, and the cross-sectional loss, μ_{loss}, of the most corroded wire is investigated.

Wang et al., [14] proposed a logarithmic correlation between the maximum pit depth and the cross-sectional loss of the most corroded wire (grey dashed line) in Fig. 2. However, due to the high scatter of experimental data, a roughly fitting was observed as confirmed by a correlation coefficient, R^2, equal to 0.49. In addition, the cross-sectional loss of the most corroded wire was limited to 33.4%.

A first new relationship between the maximum pit depth, P_{max}, and the cross-sectional loss, μ_{loss}, is presented in this paper, on the basis of a regression analyses carried out only on the data presented in this paper and in [12] by Authors (red dotted line in Fig. 2, as given by Eq. (7):

$$P_{max} = 3.4221\mu_{loss}^{0.6695} \tag{7}$$

The faithfulness of the new relationship is confirmed by a correlation coefficient, R^2, equal to 0.9765. Moreover, differently from the experimental campaign carried out by Wang et al., [14], the measured experimental data in terms of cross-sectional loss of the most corroded wire is extended to 69.20%.

In alternative, a second new relationship between the maximum pit depth, P_{max}, and the cross-sectional loss, μ_{loss}, is presented in this paper, on the basis of a regression analyses carried out on both the data presented in this paper and in [12] by Authors and the data presented by Wang et al., [14] (black dotted line in Fig. 2), as given by Eq. (8):

$$P_{max} = 3.9262\mu_{loss}^{0.5852} \tag{8}$$

Even if the accuracy of the prediction obtained with Eq. (8) is affected by the scatter of the data measured by Wang et al., [14], a significant increase of the population of data and an improvement in terms of correlation coefficient, R^2, which changed from 0.49 to 0.61, is obtained by adopting the second new relationship. The following hypothesis can be formulated in order to explain the scatter of data measured by Wang et al., [14]: (i) a different type of corrosion process – artificial climate condition – was adopted for the study of corroded prestressing strands, and (ii) a manual procedure was used to measure the maximum pit depth, that probably led to higher scatter of data if compared to the procedure adopted in the present work that is supported by the use of a laser scanner measurement technique.

4. Tensile tests on corroded strands

4.1. Experimental setup

After the measurements of the morphology of pits, tensile tests on 18 corroded prestressing strands and 4 un-corroded prestressing strands have been carried out. The tensile tests have been conducted by using a universal testing machine with maximum capacity of 250 kN, Fig. 1. The two ends of the strands have been held by the grips through epoxy resin, moulded into steel tubes, in order to accurately avoid any damage of these end parts of the specimens during loading. Then, samples have been loaded up to failure by displacement control procedure with photo recording at each time step. After the tests, the strain field of each sample has been estimated through Digital Image Correlation (DIC) analysis. To this aim, before testing, the samples have been coloured in white, and a high-contrast black speckle pattern has been applied along the overall length of the prestressing strand samples. Constant illumination has been provided during the entire test and a high-resolution digital camera Nikon D90 has been used to take photos. The post-processing phase has been carried out by using the open source software package Ncorr [22,23], which is implemented in MATLAB environment. The comparison between the reference image of the un-loaded specimen and the images of the deformed specimen - captured at each load step - has allowed to evaluate the strain field of each tested sample.

4.2. Tensile tests results

The averages values of the tensile test results of the 4 un-corroded prestressing strands are used for the mechanical properties of the

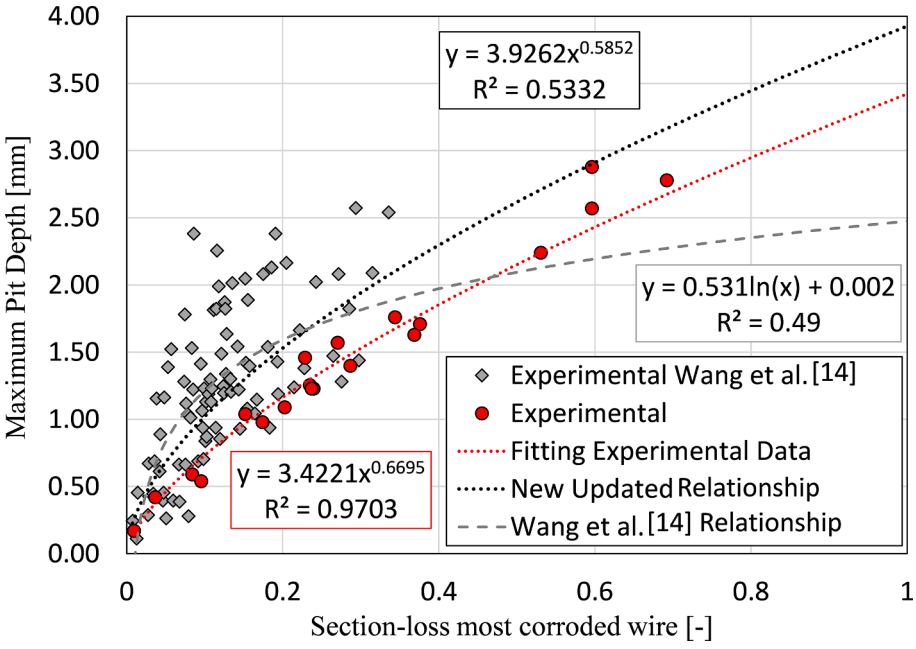

Fig. 2. Correlation between maximum pit depth and section loss of most corroded wire.

reference un-corroded strand. As a result, the ultimate strength, $f_{pu,0}$, and strain, $\varepsilon_{pu,0}$, of the un-corroded samples are equal to 1901.75 MPa and 5.1%, respectively. Then, according to the stress–strain relationship proposed by Ramberg-Osgood for prestressing strands [24], Fig. 3(b), the strength at the end of the linear branch, $f_{pp,0}$, is assumed equal to 0.7 times the ultimate strength, $f_{pu,0}$. Therefore, the strength $f_{pp,0}$ is equal to 1331.22 MPa, while the corresponding strain, $\varepsilon_{pp,0}$ results equal to 0.683% from the ratio between $f_{pp,0}$ and the Young modulus, $E_{s,0}$, set equal to 195 GPa. Finally, the yield strength, $f_{py,0}$, results equal to 1677.25 MPa and is estimated as the average value measured from the tensile tests results at an imposed strain, $\varepsilon_{py,0}$, equal to 1%. Then, an experimental ratio between yield, $f_{py,0}$, and ultimate strength, $f_{pu,0}$, equal to 0.882 is calculated.

Fig. 3(a) shows the comparison between the proposed approximated stress–strain relationship based on the Ramberg-Osgood constitutive law and the four tensile tests results carried out on un-corroded prestressing strands [24]. As it is visible, a good approximation of the experimental outcomes is obtained. Based on Fig. 3, the stress–strain curve of the un-corroded prestressing strand can be divided into three phases: (i) a first elastic phase - from 0,0 to $\varepsilon_{pp,0}$, $f_{pp,0}$ - , (ii) a transient yielding phase - from $\varepsilon_{pp,0}$, $f_{pp,0}$ to $\varepsilon_{py,0}$, $f_{py,0}$ -, and (iii) a hardening phase - from $\varepsilon_{py,0}$, $f_{py,0}$ to $\varepsilon_{pu,0}$, $f_{pu,0}$.

Fig. 4 shows the stress–strain responses of the corroded strands presented in Table 1. A constant value is assumed for the modulus of elasticity, $E_{s,0}$, as previously observed by Zhang et al., [7], because its value is strictly related to the material and it is not dependent on the pit morphology and on the damage level. On the other hand, a significant decrease of the ultimate strength and the ultimate strain is observed as the corrosion level and the cross-sectional loss increases.

Based on the experimental evidence, the most corroded wire generally broke earlier than the other external wires. Since a uniform distribution of stresses has been assumed in each wire, the failure of a wire caused a sudden drop off in the resistance of strand, which approximately resulted equal to a strength reduction of about 1/7 of the total tensile strength. In the present study, even if the corroded strand has been characterised by a residual capacity after the rupture of the first wire, the failure of the whole strand is assumed to correspond with the failure of the first, most corroded, wire. Hence, the values of the ultimate strength, $f_{pu,corr,\exp}$, and ultimate strain, $\varepsilon_{pu,corr,\exp}$ of a corroded prestressing strand are evaluated in correspondence of the occurrence of the first drop off in the stress–strain relationship, Fig. 4, as reported in Table 2. As shown in Fig. 4 and Table 1, as the corrosion level increases, the length of the hardening branch decreases. When the hardening branch disappeared, a significant brittle failure of the corroded prestressing strand took place. In this regard, the tensile behaviour of the corroded strands is subdivided in two groups, as reported in Table 2: (a) the plastic behaviour, ELA/PLA, characterised by the elastic phase (i), the yielding phase (ii) and the hardening phase (iii), or (b) the brittle behaviour, ELA, characterised by the elastic phase (i) and the yielding phase (ii) or the elastic phase (i) only.

4.3. Analysis of results

4.3.1. Ultimate strength and ultimate strain of corroded prestressing strands

The dependency of the decay of mechanical properties versus both the mass-loss of prestressing strand and the cross-sectional loss of prestressing strand is presented. To enable the comparisons among the experimental outcomes available in literature and the data presented in this paper, Fig. 5 shows the dimensionless values of the ultimate strength and the ultimate strain, calculated as the ratio between the values obtained for corroded and un-corroded specimens. Fig. 5 highlights that the experimental data presented in this paper fall within the cloud of data collected in the database; this highlights that the presented results are coherent with respect to the outcomes available in the scientific literature.

Fig. 5(a)-(b) shows the relative ultimate strength and the relative ultimate strain values, in function of the prestressing strand mass-loss, collected in the database: with red markers the data presented in this paper are plotted, whereas grey markers represent the data obtained by Zhao et al., [15].

Fig. 5(c)-(d) shows the relative ultimate strength and the relative ultimate strain values, in function of the prestressing strand cross-sectional loss, collected in the database: with red markers the data presented in this paper are plotted, whereas grey markers are used for the data presented by Jeon et al., [1,10].

Fig. 5 shows that the relative ultimate strength values can be fitted by a linear function of the mass-loss or the cross-sectional loss of the corroded strand. On the other hand, the decay of the relative ultimate strain can be fitted by an exponential function. Hence, for a given mass-loss value, the decay of the ultimate strain is considerably higher than the decay of the ultimate strength. For instance, for a 15% mass loss, a 30% decay of the ultimate strength and a 80% decay of the ultimate strain values are measured, respectively.

Similar outcomes are arising by referring to the cross-sectional loss of a corroded strand, Fig. 5(c)-(d). Considering a 30% reduction of cross-sectional loss, a 20% and 85% decay of the ultimate strength and

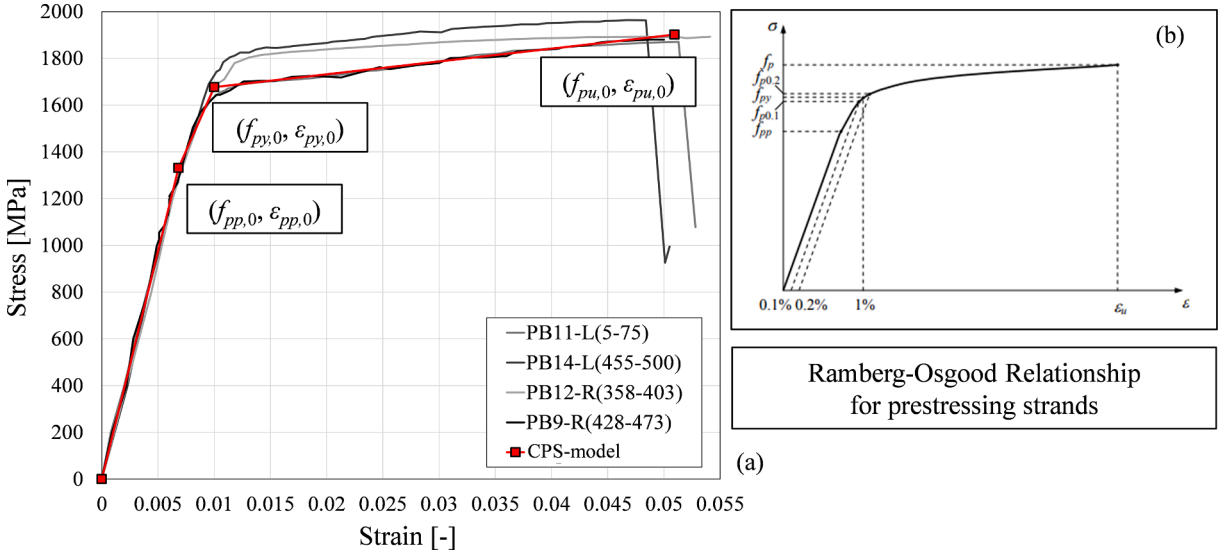

Fig. 3. Un-corroded samples: (a) tensile tests and analytical approximation; (b) Ramberg-Osgood Relationship.

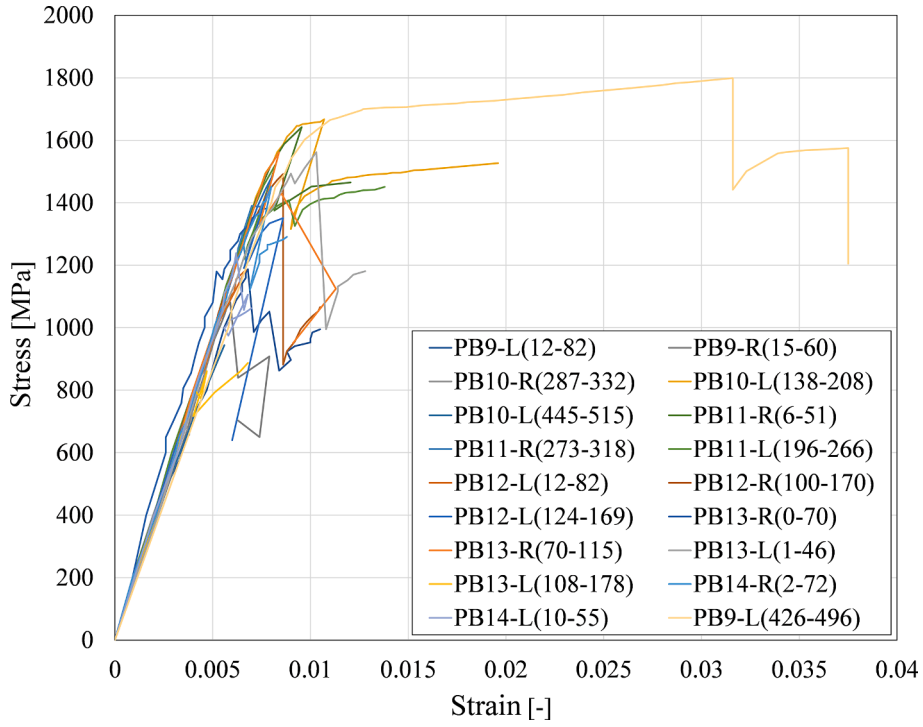

Fig. 4. Tensile tests of corroded samples: stress–strain response evaluated through DIC analysis.

Table 2
Experimental tensile test outcomes: tensile behaviour, ultimate strength, and ultimate strain.

Sample ID°	Type of failure	$f_{pu,corr,\ exp}$ [MPa]	$\varepsilon_{pu,corr,\ exp}$[-]
PB9-L(426–496)	ELA/PLA	1799.00	0.0316
PB9-R(15–60)	ELA	1082.00	0.0059
PB9-R(428–473)	ELA/PLA	1880.00	0.05
PB10-L(138–208)	ELA/PLA	1667.00	0.01
PB10-L(445–515)	ELA	944.03	0.0058
PB10-R(287–332)	ELA	1075.00	0.0045
PB11-L(5–75)	ELA/PLA	1871.00	0.0513
PB11-L(196–266)	ELA	1516.00	0.0082
PB11-R(6–51)	ELA	1642.00	0.0088
PB11-R(273–318)	ELA	1387.00	0.0075
PB12-L(12–82)	ELA	1185.00	0.0069
PB12-L(124–169)	ELA	1491.00	0.0081
PB12-R(100–170)	ELA	1492.00	0.0086
PB12-R(358–403)	ELA/PLA	1893.00	0.0541
PB13-L(1–46)	ELA/PLA	1562.00	0.0103
PB13-L(108–178)	ELA	800.00	0.0041
PB13-R(0–70)	ELA	1381.00	0.0077
PB13-R(70–115)	ELA	1562.00	0.0089
PB14-L(10–55)	ELA	1239.00	0.0079
PB14-L(455–500)	ELA/PLA	1963.00	0.0484
PB14-R(2–72)	ELA	1452.00	0.0075

ultimate strain are measured, respectively.

Therefore, experimental results show that the decay in the ultimate strain is generally more relevant compared to the decay in the ultimate strength, leading to significant consequences for ductility of corroded PC members, often characterised by brittle failures.

4.4. Dependency of mechanical properties decay on pit type morphology

As discussed in section 4.2, the un-corroded samples failed after a significant plastic deformation at the hardening stage (see Fig. 3(a)). On the other hand, as the cross-sectional loss increases, the hardening phase decreases till a threshold limit characterised only by the elastic and yielding phases as evidenced in Fig. 4. The value of this latter critical limit of the cross-sectional loss of the most corroded wire, μ_{lim}, that causes brittle failure is determined by coupling the finite element analysis (FEM) results proposed by Jeon et al., [10] with the experimental data presented in this paper. To this aim, the relationship between the relative ultimate strain and the cross-sectional loss, μ_{loss}, of the most corroded wire is analyzed for the different pit type morphologies, as show in Fig. 6.

The green and orange markers in Fig. 6 represent experimental data of most corroded wires belonging to strands that exhibited failures in the plastic and in the elastic branch, respectively, Table 2. Generally, two different exponential trends can be used to describe the reduction of the ultimate strain for different levels of cross-sectional loss. In correspondence of the intersection point between the two different exponential trends, the critical value of the cross-sectional loss, μ_{lim}, is evaluated. The critical value, μ_{lim}, results equal to 8.1%, 10.7%, and 5.4% for pit type morphology 1, 2, and 3, respectively. It is worth noting that this critical point, μ_{lim}, plays a fundamental role in the overall description of the stress–strain response of a corroded strand, since it governs the presence of the hardening phase.

Basically, the first exponential trend, illustrated in Fig. 6, for cross-sectional loss values lower than the critical value, μ_{lim}, is characterised by a significant reduction of ultimate strain values. Otherwise, the second exponential trend, illustrated in Fig. 6, for cross-sectional loss values higher than the critical value, μ_{lim}, is characterised by a less relevant reduction because the resulting ultimate strain lies on the elastic branch of the stress–strain relationship, as observed by Wang et al., [14].

Jeon et al., [10] evaluated the capacity of corroded strands on the basis of the response of the seven wires; the response of each wire was predicted from non-linear finite element analyses where the different pit type morphologies - denoted as type 1, type 2 and type 3 in Fig. 1 - were modelled.

Fig. 7 shows the relationship between the relative ultimate strength, $f_{pu,corr}$, and the cross-sectional loss, μ_{loss}, numerically obtained by Jeon et al., [10] and the experimental results obtained in this paper by tensile tests. Additionally, new formulations for the assessment of the ultimate strength provided by Eq. (9), Eq. (10) and Eq. (11) for the pit type morphology 1, 2, and 3, respectively, are proposed. The most relevant

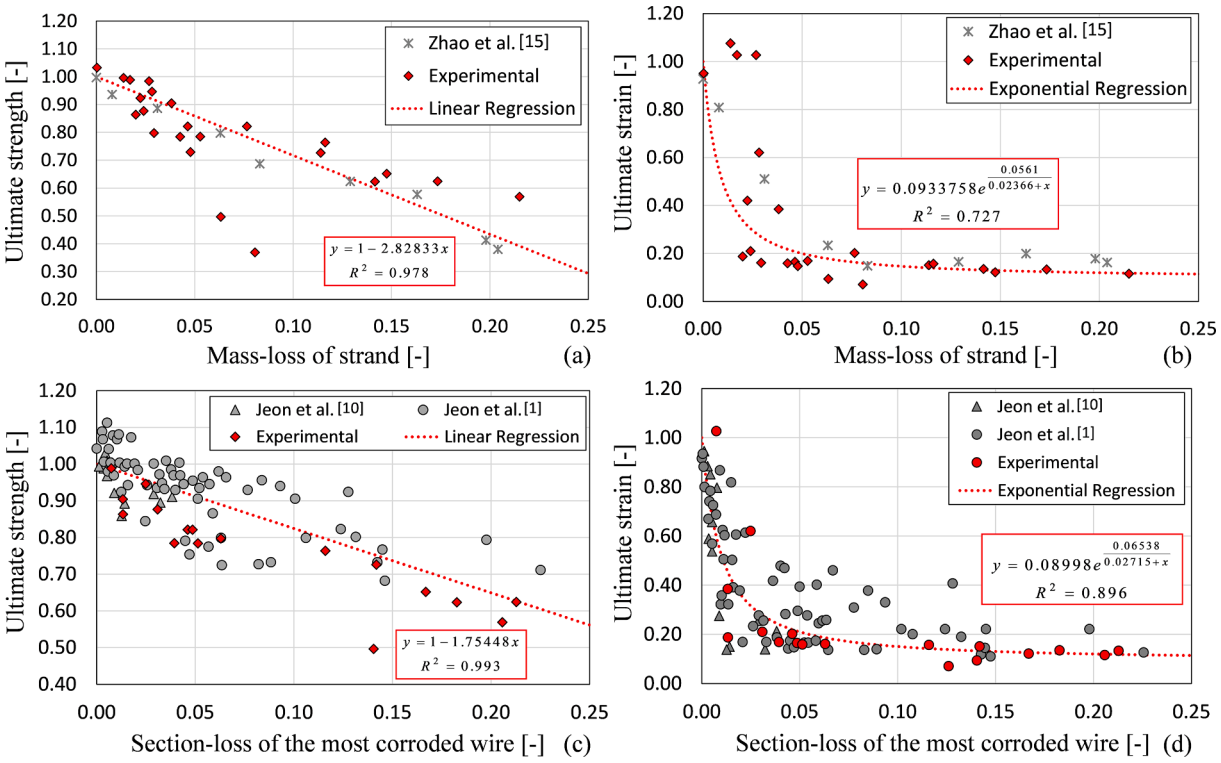

Fig. 5. Relative ultimate strength and relative ultimate strain variation as a function of mass loss (a), (b) and cross-sectional loss of a prestressing strand (c), (d).

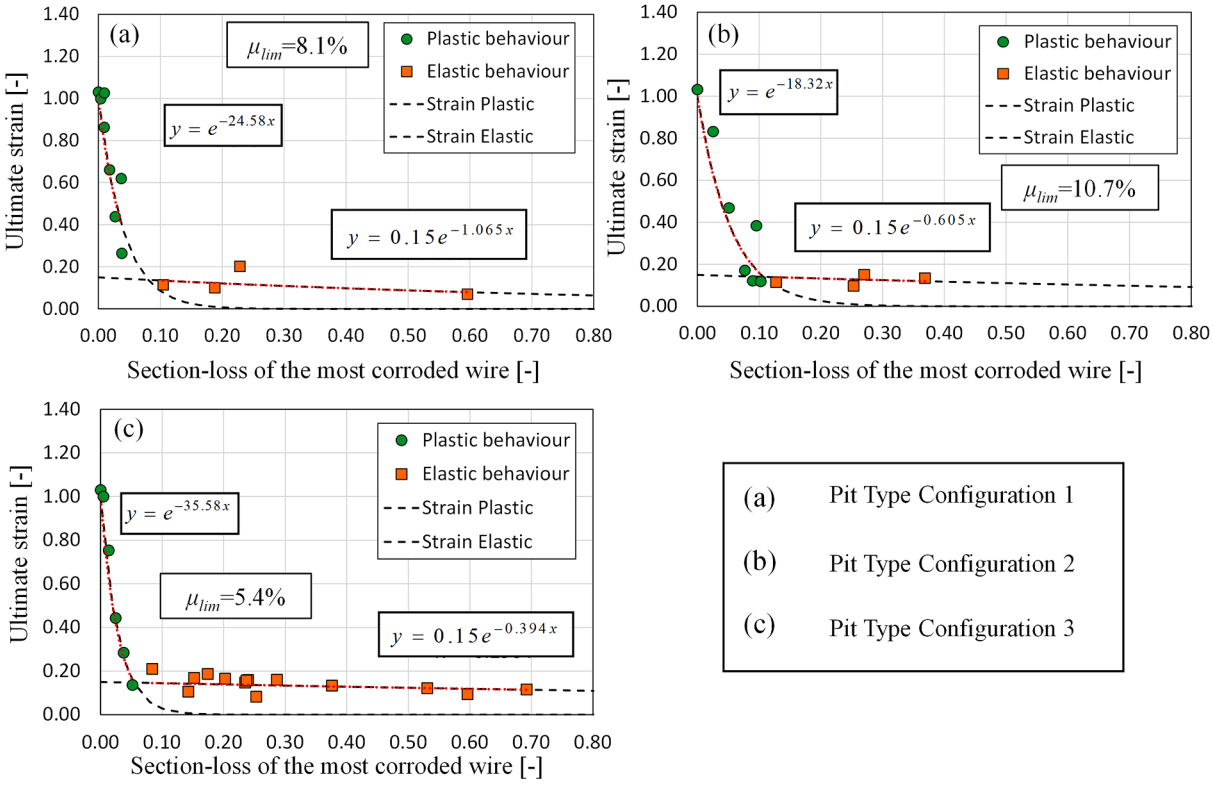

Fig. 6. Reduction of relative ultimate strain for different pit type morphologies.

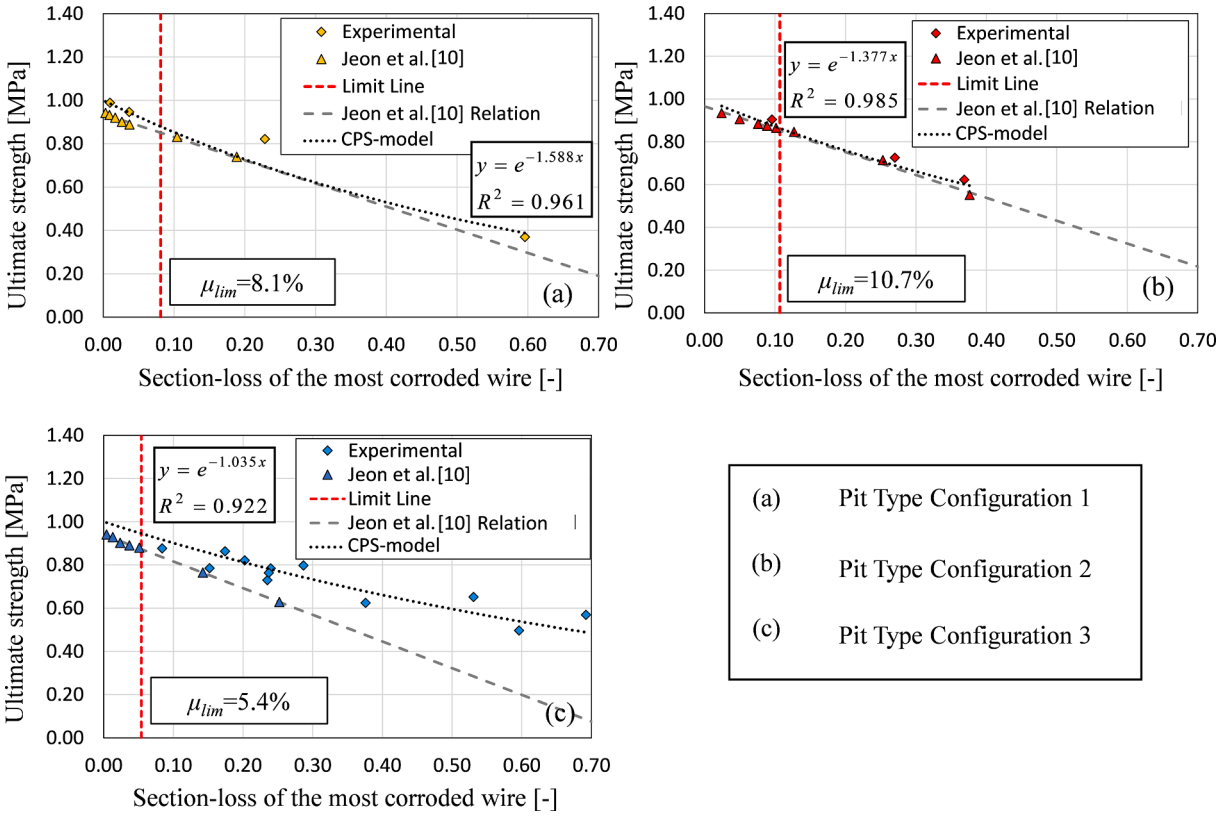

Fig. 7. Reduction of ultimate strength for different pit type morphologies.

modifications made to the formulation proposed by Jeon et al., [10] are illustrated in the following: (a) interpolation of the available data by means of exponential relations instead of the linear relation, and (b) set - for a cross-sectional loss, μ_{loss}, equal to 0% - the value of the ultimate strength equal to the value of the un-corroded strand regardless of the pit type morphology taken into account. The good agreement of the fitting regression analyses with experimental outcomes is confirmed by a correlation coefficient, R^2, equal to 0.961, 0.985, and 0.922 for the pit type morphology 1, 2, and 3, respectively.

In Fig. 7(a)-(c), the dashed grey line and the dotted black line represent the formulations proposed by Jeon et al., [10] and by the CPS-model presented in this study, respectively. At the same time, the red dashed line stands for the critical value of the cross-sectional loss, μ_{lim}, beyond which the hardening phase (iii) disappears, and the tensile response is characterised by the presence of the elastic phase (i) and the yielding phases (ii), only.

$$\frac{f_{pu,corr}}{f_{pu,0}} = e^{-1.588\mu_{loss}} \tag{9}$$

$$\frac{f_{pu,corr}}{f_{pu,0}} = e^{-1.377\mu_{loss}} \tag{10}$$

$$\frac{f_{pu,corr}}{f_{pu,0}} = e^{-1.035\mu_{loss}} \tag{11}$$

5. A constitutive model for corroded prestressing strands (CPS-model)

5.1. Basic assumptions

The main assumptions of the proposed constitutive model for corroded prestressing strands (named CPS-model) presented in this paper are listed in the following:

- The response of the strand is given by the sum of the contribution of wires working as springs in parallel. The contributions provided by each wire is evaluated in correspondence of the section characterised by the maximum pit depth, P_{max}.
- The tensile resistance of each wire is obtained by multiplying the reduced strength of each wire time the un-corroded section of each wire.
- Pits are classified according to the three pit type morphologies proposed by Jeon et al., [10] and the area loss is calculated according to Eqs.(2)-(4) depending on the maximum pit depth, P_{max}.
- The inner wire is assumed un-corroded. The cross-sectional loss of external wires, μ_{loss}, is calculated according to Eq. (6).
- Three different formulations are given in Eqs.(9)-(11) to calculate the ultimate strength depending on cross-sectional loss, μ_{loss}, for the three different pit type morphologies, respectively.
- The ultimate strength of strands is fixed in correspondence of the ultimate strength of the most corroded wire, Appendix A.
- The stress–strain curve of each un-corroded or slightly corroded wire is estimated by assuming the tri-linear Ramberg-Osgood model, as illustrated in Fig. 8 for un-corroded prestressing strand.
- For cross-sectional loss of the corroded wire, μ_{loss}, higher than the critical value, μ_{lim}, the hardening phase disappears, while the presence of the yielding phase depends on the ultimate strength value, $f_{pu,corr}$. If $f_{pu,corr}$ is higher than the stress at the end of the elastic stage, $f_{pp,0}$, the yielding stage develops, and the stress–strain relations of a corroded wire can be expressed by a bi-linear model. Otherwise, the stress–strain response of the corroded wire is characterised by the presence of the elastic phase only, as shown in Fig. 8.
- The elastic ($E_{s,0}$), yielding ($E'_{s,0}$), and hardening ($E''_{s,0}$) modulus are assumed not to change due to corrosion deterioration process and are set equal to their un-corroded value. Consequently, starting from the predicted ultimate strength value, $f_{pu,corr}$, the corresponding ultimate strain, $\varepsilon_{pu,corr}$, is estimated.

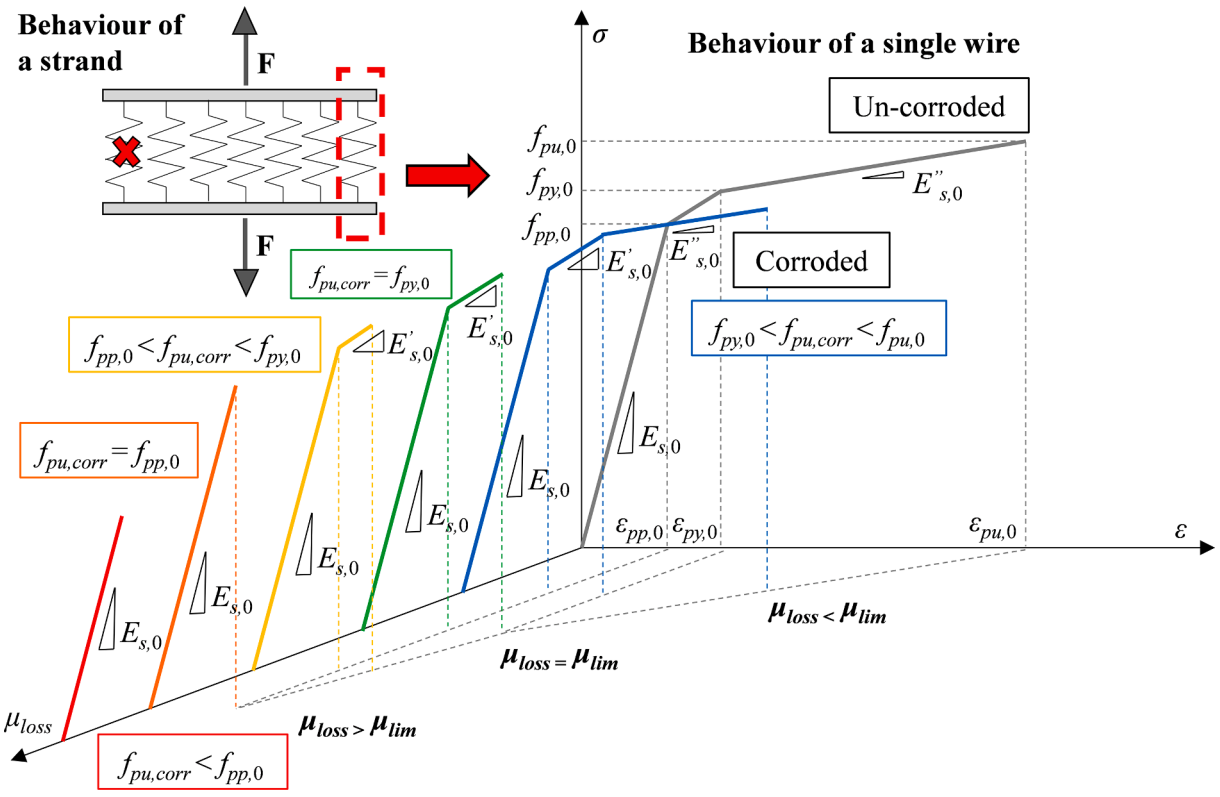

Fig. 8. Stress–strain behaviour of a corroded wire as a function of the cross-sectional loss.

5.2. Stress–strain relationship for un-corroded wire

The ultimate strength, $f_{pu,corr}$, of each wire is estimated through Eqs. (9)-(11) as a function of the pit type morphology and the cross-sectional loss. Thereafter, according to the Ramberg-Osgood model, the stress at the end of the elastic stage, $f_{pp,0}$, as well as the yield stress, $f_{py,0}$, are defined, respectively, through the expressions provided by Eq. (12) and Eq. (13) as a function of the un-corroded ultimate strength, $f_{pu,0}$.

$$f_{pp,0} = 0.7 f_{pu,0} \tag{12}$$

$$f_{py,0} = 0.882 f_{pu,0} \tag{13}$$

Since the corrosion deterioration process does not affect the elasticity modulus, $E_{s,0}$, the un-corroded value equal to 195 GPa is considered. The elastic stage is completely defined once the strain at end of the elastic stage, $\varepsilon_{pp,0}$, is calculated through Eq. (14). Referring to the yielding stage, the yield strain, $\varepsilon_{py,0}$, is set equal to 1% according to the constitutive law proposed by Ramberg and Osgood, Fig. 4(b).

$$\varepsilon_{pp,0} = \frac{0.7 f_{pu,0}}{E_s} = \frac{f_{pp,0}}{E_s} \tag{14}$$

Based on the previous assumptions, the stress–strain behaviour of an un-corroded wire can be expressed as described in Eq. (15):

$$\sigma_w(\varepsilon) = \begin{cases} \varepsilon E_{s,0} & \varepsilon \le \varepsilon_{pp,0} \\ \varepsilon_{pp,0} E_{s,0} + E'_{s,0}\left(\varepsilon - \varepsilon_{pp,0}\right) & \varepsilon_{pp,0} < \varepsilon \le \varepsilon_{py,0} \\ \varepsilon_{pp,0} E_{s,0} + E'_{s,0}\left(\varepsilon_{py,0} - \varepsilon_{pp,0}\right) + E''_{s,0}\left(\varepsilon - \varepsilon_{py,0}\right) & \varepsilon_{py,0} < \varepsilon \le \varepsilon_{pu,0} \\ 0 & \varepsilon > \varepsilon_{pu,0} \end{cases} \tag{15}$$

where $\sigma_w(\varepsilon)$ is defined as the stress of a wire with respect to a given ε, while $E'_{s,0}$, $E''_{s,0}$ are the un-corroded yielding and hardening modulus, calculated according to Eq. (16) and Eq. (17), that results equal to 109 GPa and 5.47 GPa, respectively, as reported in Fig. 8.

$$E'_{s,0} = \frac{f_{py,0} - f_{pp,0}}{\varepsilon_{py,0} - \varepsilon_{pp,0}} \tag{16}$$

$$E''_{s,0} = \frac{f_{pu,0} - f_{py,0}}{\varepsilon_{pu,0} - \varepsilon_{py,0}} \tag{17}$$

5.3. Stress–strain relationship for corroded wire

The ultimate strength, $f_{pu,corr}$, of the corroded wire is estimated by Eqs (9)-(11); then the corresponding ultimate strain, $\varepsilon_{pu,corr}$, is estimated through Eq. (18) in function of both the actual cross-sectional loss, μ_{loss}, and the critical value of cross-sectional loss, μ_{lim}, associated to the pit type morphology of the investigated wire.

$$\varepsilon_{pu,corr} = \begin{cases} \mu_{loss} < \mu_{lim} & \varepsilon_{py,0} + \dfrac{f_{pu,corr} - f_{py,0}}{E''_{s,0}} \quad f_{py,0} < f_{pu,corr} \le f_{pu,0} \\ \mu_{loss} \ge \mu_{lim} & \begin{cases} \varepsilon_{pp,0} + \dfrac{f_{pu,corr} - f_{pp,0}}{E'_{s,0}} & f_{pp,0} < f_{pu,corr} \le f_{py,0} \\ \dfrac{f_{pu,corr}}{E_{s,0}} & f_{pu,corr} < f_{pp,0} \end{cases} \end{cases} \tag{18}$$

Finally, based on the corroded ultimate strain, $\varepsilon_{pu,corr}$, evaluated through Eq. (18), the stress–strain behaviour of a corroded wire can be summarised as expressed in Eq. (19):

$$\sigma_w(\varepsilon)=\begin{cases}\mu_{loss}<\mu_{lim} & \begin{cases}\varepsilon E_{s,0} & \varepsilon\le\varepsilon_{pp,0}\\ \varepsilon_{pp,0}E_{s,0}+E'_{s,0}\left(\varepsilon-\varepsilon_{pp,0}\right) & \varepsilon_{pp,0}<\varepsilon\le\varepsilon_{py,0}\\ \varepsilon_{pp,0}E_{s,0}+E'_{s,0}\left(\varepsilon_{py,0}-\varepsilon_{pp,0}\right)+E''_{s,0}\left(\varepsilon-\varepsilon_{py,0}\right) & \varepsilon_{py,0}<\varepsilon\le\varepsilon_{pu,corr}\\ 0 & \varepsilon>\varepsilon_{pu,corr}\end{cases}\\ \mu_{loss}\ge\mu_{lim} & \begin{cases}\begin{cases}\varepsilon E_{s,0} & \varepsilon\le\varepsilon_{pp,0}\\ \varepsilon_{pp,0}E_{s,0}+E'_{s,0}\left(\varepsilon-\varepsilon_{pp,0}\right) & \varepsilon_{pp,0}<\varepsilon\le\varepsilon_{pu,corr}\\ 0 & \varepsilon>\varepsilon_{pu,corr}\end{cases}\\ \begin{cases}\varepsilon E_{s,0} & \varepsilon\le\varepsilon_{pu,corr}\\ 0 & \varepsilon>\varepsilon_{pu,corr}\end{cases}\end{cases}\end{cases}\tag{19}$$

The tensile behaviour of the strand is obtained by adopting the equivalent spring material model proposed by Jeon et al., [10] as given by Eq. (20):

$$\sigma(\varepsilon)=\frac{\sum_{i=1}^{7}\left(\sigma_{w,i}(\varepsilon)A_{p0,i}\right)}{\sum_{i=1}^{7}\left(A_{p0,i}\right)}\tag{20}$$

where $\sigma_{w,i}$ and $A_{p0,i}$ are the stress and the cross-sectional area of the ith wire making up the strand.

5.4. Comparisons between analytical and experimental results

The analytical response of sample PB9-L(12–82) obtained by adopting the CPS-model (red curve) is compared in Fig. 9 with the experimental response (black curve) and with the analytical response obtained by adopting the model presented by Jeon at al. [10] (green curve). Fig. 9 shows that the rupture of the first wire takes place in correspondence of the most corroded section - evaluated by using GOM Inspect software -, where the maximum pit depth has been measured. The analytical responses after the failure of the first wire are plotted with dotted lines to highlight that the CPS-model can detect the sequence of failures occurring in each wire but that for safety reasons the maximum tensile resistance of the strand is achieved in correspondence of the failure of the most corroded wire.

Since the cross-sectional loss, μ_{loss}, of sample PB9-L(12–82) is higher than the critical value of cross-sectional loss, μ_{lim}, the failure of the most corroded wire occurs in the elastic phase (i).

The elongation has been measured by means of an axial extensometer with gauge length equal to 25 mm to assess the accuracy and reliability of DIC results, as shown in Fig. 9 and Fig. 10. However, the axial extensometer has been removed at a relative early load stage to avoid instrumental damages and to ensure the safety of workers in the case of a sudden strand rupture. The obtained outcomes show a good correlation between the modulus of elasticity estimated by performing DIC analysis and the modulus of elasticity evaluated using the axial extensometer. Fig. 9 shows that the value of the modulus of elasticity of the corroded strand can be assumed equal to the value of the modulus of elasticity of the un-corroded strand, as assumed in paragraph 5.1.

5.5. Validation of the proposed model

In Fig. 10 the applicability and the accuracy of the proposed CPS-model is verified by comparing the analytical stress–strain curves with the experimental results and with the analytical results obtained by using the Jeon et al., [10] proposal.

Appendix A reports the measured values of cross-sectional loss of each wire and the classification of pits for all the corroded prestressing samples in correspondence of the section where the maximum pit depth, P_{max}, has been measured.

The stress–strain curves reported in Fig. 10 highlight the good agreement between the experimental results and the predicted values of the ultimate strength and the ultimate strain. Corroded specimens reveal a reduction in ductility and strength that are properly simulated by the CPS-model. Continuous lines are reported up the failure of the first wire to compare the experimental and the analytical maximum strength values of the analysed strands. The analytical model is also able to predict the post-peak tensile resistance of the analysed strands - plotted with dotted lines - and the sequence of failure of the wires.

Fig. 11(a) shows the comparison between the dimensionless ratio of the experimental and the numerical ultimate strength obtained by adopting the proposed CPS-model and the model proposed by Jeon et al., [10]. Fig. 11(b) shows the comparison between the dimensionless ratio of the experimental and the numerical ultimate strain obtained by adopting the proposed CPS-model and the model proposed by Jeon et al., [10]. Fig. 11 highlights that the CPS-model provides a better approximation of the mechanical properties than the model proposed by Jeon et al., [10].

Indeed, by excluding just one sample out of range, the ratio between experimental and analytical ultimate strength - predicted by CPS-model - range from 0.92 to 1.17, while the ratio between the experimental and the analytical ultimate strain range from 0.91 to 1.40. On the other hand, the same ratios evaluated by using the Jeon et al., [10] model range from 1.00 to 1.27 and from 0.90 to 1.60, respectively. Even if a good agreement between experimental outcomes and analytical predictions is obtained by using the CPS-model, for some samples a slightly overestimations is observed.

The dimensionless ratios reported in Fig. 11 are statistically treated to calculate the average value, the standard deviation, and the coefficient of variation (COV), as reported in Table 3.

Based on the obtained results, the CPS-model provides a better

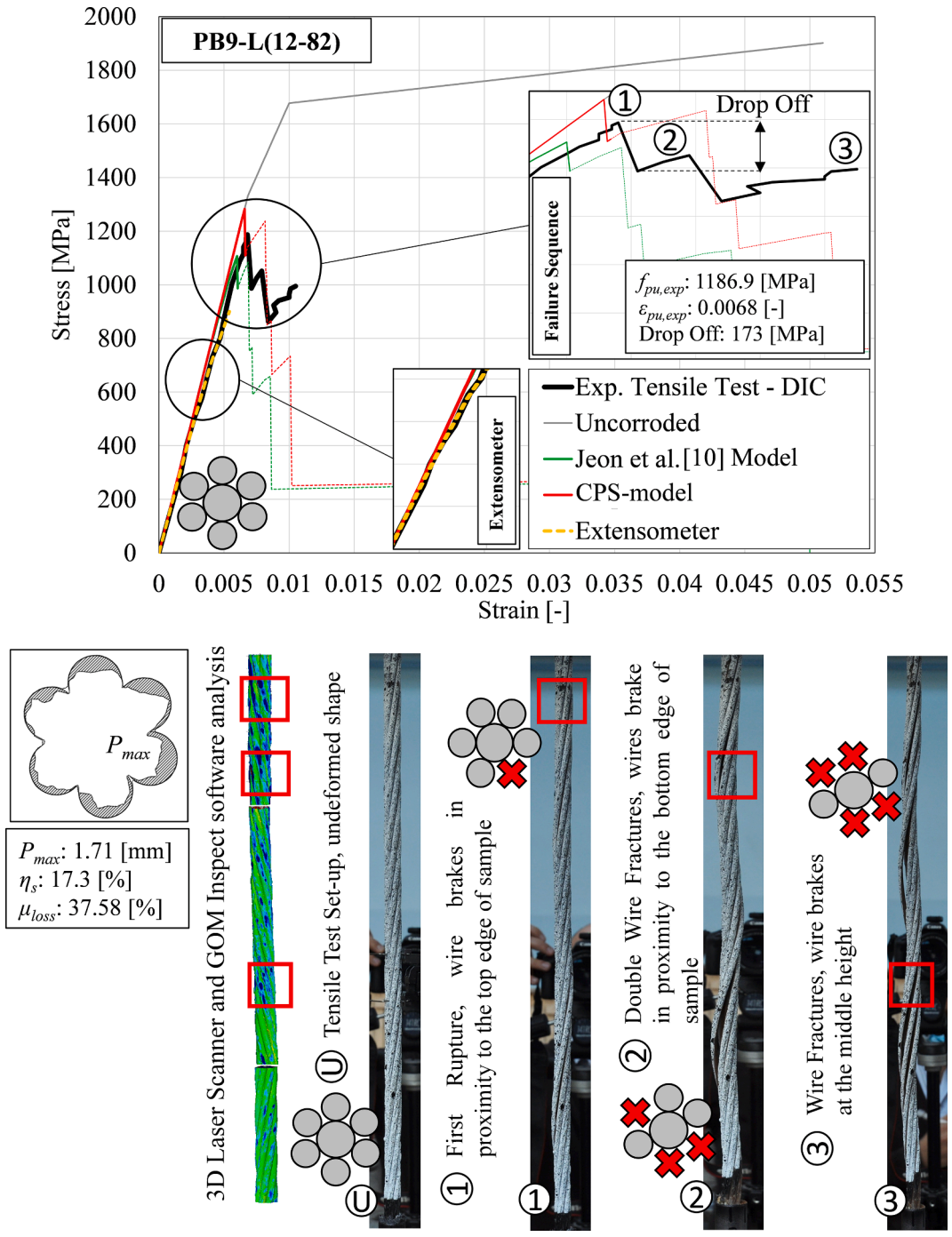

Fig. 9. PB9-L(12–82): comparison between experimental and analytical stress–strain responses. The failure sequence of the wires has been superimposed on the figures.

approximation than the model proposed by Jeon et al., [10] - both in terms of the average value and standard deviation - for both the ultimate strength ratios and the ultimate strain ratios. Furthermore, a relevant improvement in the prediction of the ultimate strain can be achieved by using the CPS-model. Indeed, a similar coefficient of variation, COV, is calculated for the ultimate strength ratio, which results equal to 0.111 and 0.109 by adopting the CPS-model and the model proposed by Jeon et al., [10], respectively. On the other hand, the COV calculated for the ultimate strain ratio, results equal to 0.147 and 0.177 by adopting the same two models, respectively.

6. Conclusions

In the present work, a constitutive model, named CPS-model, for prestressing strands subjected to pitting corrosion induced by chloride attack is proposed. To this aim, 24 prestressing strand samples (4 uncorroded and 20 corroded) are analysed. Firstly, the mass loss of each sample is measured according to the ASTM G1-03 Standard. Then, fundamental parameters such as, maximum pit depth and cross-sectional loss are estimated by performing a 3D laser scanner procedure and by carrying out the post-processing of data by means of GOM Inspect software. Thereafter, each corroded wire is classified according to the three different pit type morphologies. Then, for each pit type

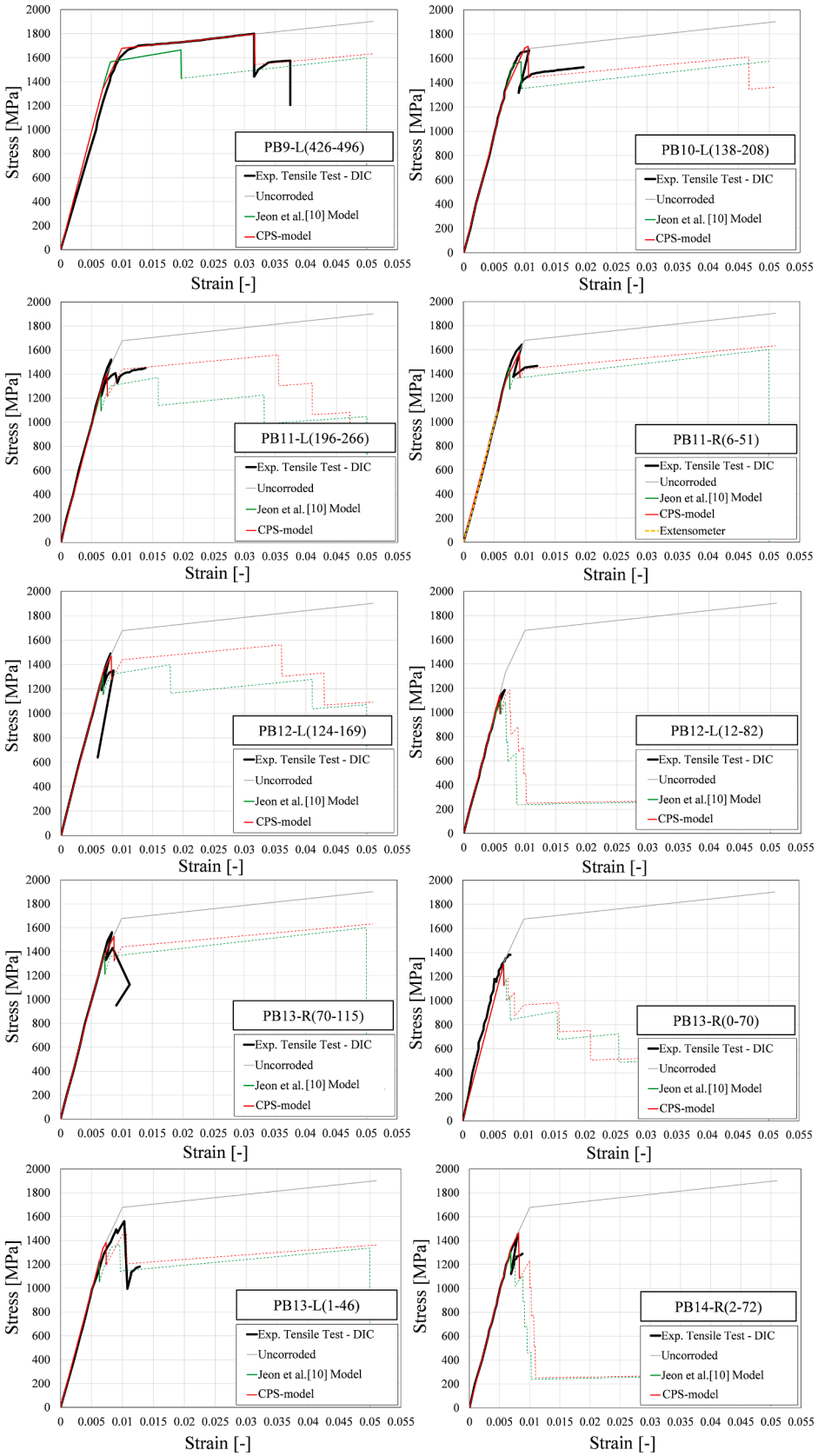

Fig. 10. Comparison between experimental tensile test results (DIC analysis) and analytical models: (i) CPS-model, red line, and (ii) Jeon et al., [10] model, green line. (For interpretation of the references to colour in this figure legend, the reader is referred to the web version of this article.)

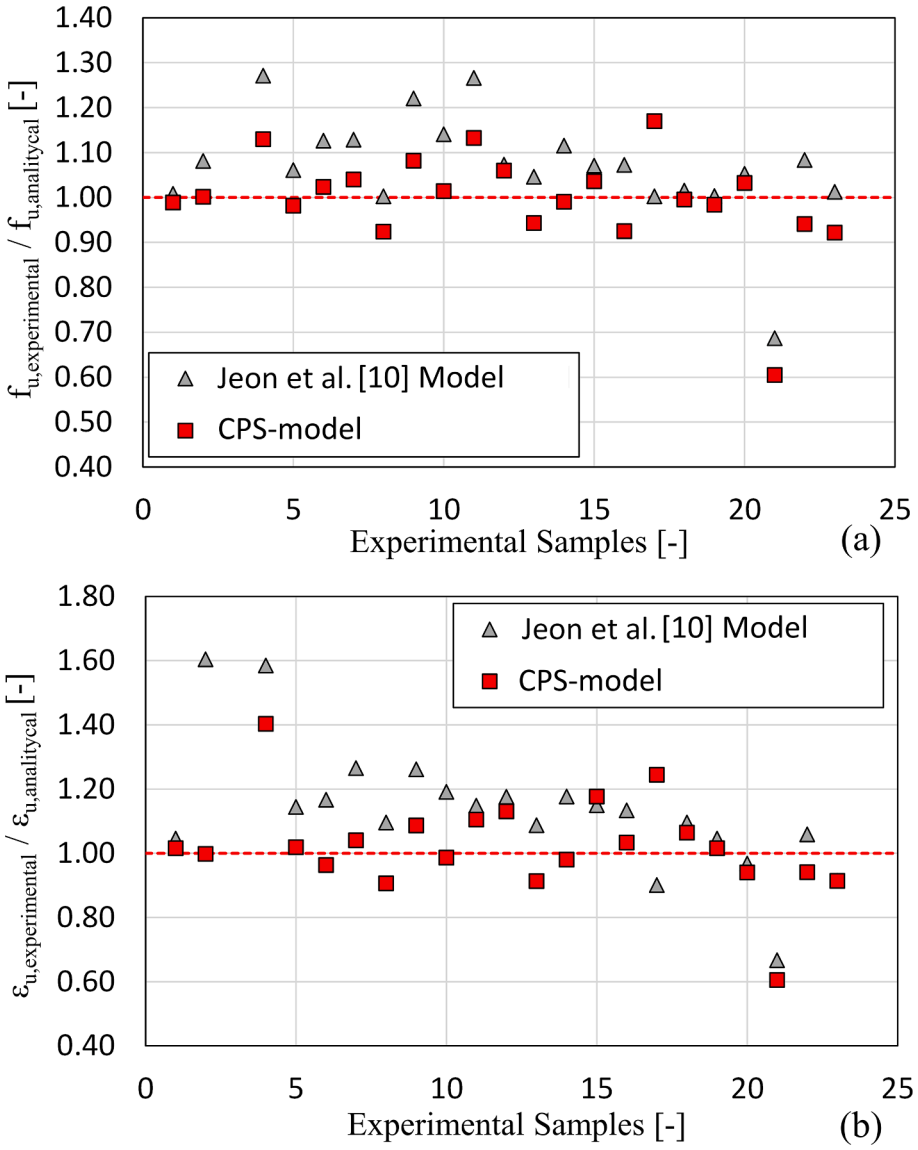

Fig. 11. Dimensionless ratio between experimental and numerical outcomes in terms of: (a) ultimate strength, and (b) ultimate strain.

morphology, the critical cross-sectional loss, corresponding to the loss of the hardening branch in the stress–strain response, is evaluated. Based on the experimental tensile test results, regression analyses on the variation of the ultimate strength and ultimate strain of corroded prestressing strands as a function of corrosion level are conducted. Finally, referring to the equivalent spring material model, a new constitutive model, named CPS-model, for corroded prestressing strands is introduced.

The main outcomes of the study are listed in the following:

- A database collecting the available results on maximum pit depth, ultimate strength, and ultimate strain in function of the mass-loss of strands or in function the cross-sectional loss of the most corroded wire is created. A new relationship between the maximum pit depth and the cross-sectional loss of the most corroded wire is proposed.
- Experimental tensile tests on naturally corroded prestressing strands are conducted to analyse the dependency of the ultimate strength and ultimate strain on the cross-sectional loss of the most corroded wire. A new exponential relationship for the assessment of the ultimate strength is presented - for each pit type morphologies taken into account. Moreover, the critical cross-sectional loss value - that causes the loss of the hardening phase in the response of wire - is fixed equal to 8.1%, 10.7% and 5.4% for pit type morphology 1, 2 and 3, respectively.
- A new constitutive law for corroded prestressing strands, named CPS-model, is introduced based on the assumption that the response of the strand is equivalent to the sum of the responses of the wires that behave as springs in parallel. The failure of the strand is assumed at the rupture of the most corroded wire.
- Finally, the accuracy and applicability of the proposed model is verified by comparing the experimental tensile test results with the analytical results obtained by adopting the CPS-model. The average value and the coefficient of variation (COV) of the ratio between the experimental and the analytical results is equal to 0.996 and 0.111 - with reference to the ultimate strength – and is equal to 1.022 and 0.147 with reference to the ultimate strain. The statistical analysis demonstrates that the presented method provides more accurate predictions if compared with other analytical methods available in literature.
- An operative procedure, based on in-situ sampling and measuring the maximum pit depth on the corroded wire of the strand can be established to operatively apply the outcomes of the present work to prestressing elements in service with damage due to corrosion.

Table 3
Prediction outcomes referring to: (i) Proposed CPS - model, and (ii) Jeon et al., [10] model.

Sample ID°	CPS - model		Jeon et al., model		CPS - model		Jeon et al., model	
	$f_{pu,corr}$[MPa]	$\varepsilon_{pu,corr}$[-]	$f_{pu,corr}$[MPa]	$\varepsilon_{pu,corr}$[-]	$f_{pu,corr,exp}/ f_{pu,corr}$	$\varepsilon_{pu,corr,exp}/ \varepsilon_{pu,corr}$	$f_{pu,corr,exp}/ f_{pu,corr}$	$\varepsilon_{pu,corr,exp} / \varepsilon_{pu,corr}$
PB9-L(12–82)	1282.9	0.0066	1106.6	0.0060	0.93	1.03	1.07	1.13
PB9-L(426–496)	1795.9	0.0317	1664.0	0.0197	1.00	1.00	1.08	1.60
PB9-R(15–60)	924.9	0.0047	1079.5	0.0066	1.17	1.24	1.00	0.90
PB9-R(428–473)	1901.7	0.0515	1865.0	0.0500	0.99	1.02	1.01	1.05
PB10-L(138–208)	1698.4	0.0105	1571.1	0.0094	0.98	1.02	1.06	1.14
PB10-L(445–515)	1024.3	0.0053	932.53	0.0053	0.92	0.91	1.01	0.91
PB10-R(287–332)	745.9	0.0038	648.0	0.0034	0.94	0.94	1.08	1.06
PB11-L(5–75)	1901.7	0.0515	1865.0	0.0500	0.98	1.02	1.00	1.05
PB11-L(196–266)	1401.4	0.0075	1242.3	0.0065	1.08	1.09	1.22	1.26
PB11-R(6–51)	1578.5	0.0092	1454.7	0.0076	1.04	1.04	1.13	1.26
PB11-R(273–318)	1470.7	0.0082	1326.1	0.0069	0.94	0.91	1.05	1.09
PB12-L(12–82)	1143.7	0.0059	1106.6	0.0060	1.04	1.18	1.07	1.15
PB12-L(124–169)	1470.3	0.0082	1306.8	0.0068	1.01	0.99	1.14	1.19
PB12-R(100–170)	1615.1	0.0095	1488.0	0.0079	0.92	0.91	1.00	1.10
PB12-R(358–403)	1901.7	0.0515	1865.0	0.050	1.00	1.06	1.02	1.10
PB13-L(1–46)	1382.8	0.0073	1228.9	0.0065	1.13	1.40	1.27	1.58
PB13-L(108–178)	1322.7	0.0068	1165.1	0.0062	0.60	0.60	0.69	0.67
PB13-R(0–70)	1302.8	0.0068	1286.9	0.0066	1.06	1.113	1.07	1.18
PB13-R(70–115)	1526.4	0.0087	1386.6	0.0072	1.02	0.96	1.13	1.17
PB14-L(10–55)	1093.9	0.0056	978.7	0.0054	1.13	1.11	1.27	1.15
PB14-L(455–500)	1901.7	0.0515	1865.0	0.0500	1.03	0.94	1.05	0.97
PB14-R(2–72)	1466.0	0.0082	1302.1	0.0068	0.99	0.98	1.12	1.18
Green boxes	Un-corroded samples	**Average Value**			0.996	1.022	1.07	1.131
		Standard Deviation Value			0.111	0.150	0.117	0.200
		Coefficient of Correlation, COV, Value			0.111	0.147	0.109	0.177

7. Data availability

The raw/processed data required to reproduce these findings cannot be shared at this time as the data also forms part of an ongoing study.

CRediT authorship contribution statement

Lorenzo Franceschini: Writing – original draft, Visualization, Data curation, Conceptualization. **Francesca Vecchi:** Methodology, Visualization, Data curation, Conceptualization. **Francesco Tondolo:** Supervision, Funding acquisition, Resources, Investigation. **Beatrice Belletti:** Project administration, Supervision, Writing – review & editing, Conceptualization, Funding acquisition. **Javier Sánchez Montero:** Investigation, Validation.

Declaration of Competing Interest

The authors declare that they have no known competing financial interests or personal relationships that could have appeared to influence the work reported in this paper.

Acknowledgements

The authors are grateful to the members of the ARMTech group of Politecnico di Torino for their help with all the instrumentation and the facilities to test the specimens. This paper reports the scientific results obtained by the University of Parma and by the Polytechnic of Turin within the PRIN project (Italian Research Project of Prominent National Interest): "Failure mechanisms due to lack of construction details and degradation phenomena in existing reinforced concrete buildings" financially co-founded by MIUR (Italian Ministry of Education, University and Research MIUR - grant number 2015HZ24KH).

Appendix A

Considering the 24 collected samples, the following Table reports the cross-sectional area and the geometrical classification of the pits for each external wire (six for each sample) in correspondence of the section where the maximum pit depth, P_x, has been measured. The core wire has been assumed as un-corroded.

Sample ID°	wire	μ_{loss}[%]	Pit Morphology according to Jeon et al., [10]	Sample ID°	wire	μ_{loss} [%]	Pit Morphology according to Jeon et al., [10]
PB9-L(12–82)	W_1	24.23	3	PB9-R(15–60)	W_1	7.18	3
	W_2	21.02	3		W_2	6.59	3
	W_3	11.19	3		W_3	27.40	3
	W_4	11.42	3		W_4	69.21	3
	W_5	23.42	3		W_5	18.63	2
	W_6	37.59	3		W_6	10.46	2
PB9-L(426–496)	W_1	–	0	PB9-R(428–473)	W_1	–	–
	W_2	–	0	Uncorroded	W_2	–	–
	W_3	–	0		W_3	–	–
	W_4	3.67	1		W_4	–	–
	W_5	–	0		W_5	–	–

(*continued on next page*)

(*continued*)

	W_6	–	0		W_6	–	–
PB10-L(138–208)	W_1	–	0	PB10-R(32–102)	W_1	–	–
	W_2	–	0	(NEGLECTED)	W_2	–	–
	W_3	8.39	3		W_3	–	–
	W_4	1.22	3		W_4	–	–
	W_5	–	0		W_5	–	–
	W_6	–	0		W_6	–	–
PB10-L(445–515)	W_1	1.30	1	PB10-R(287–332)	W_1	13.26	3
	W_2	–	0		W_2	–	0
	W_3	–	0		W_3	–	0
	W_4	59.61	3		W_4	7.48	1
	W_5	29.94	2		W_5	59.58	1
	W_6	–	0		W_6	1.58	3
PB11-L(5–75)	W_1	–	–	PB11-R(6–51)	W_1	17.41	3
Uncorroded	W_2	–	–		W_2	–	0
	W_3	–	–		W_3	–	0
	W_4	–	–		W_4	–	0
	W_5	–	–		W_5	–	0
	W_6	–	–		W_6	–	0
PB11-L(196–266)	W_1	–	0	PB11-R(273–318)	W_1	–	–
	W_2	4.41	3		W_2	–	–
	W_3	28.66	3		W_3	23.52	3
	W_4	2.81	3		W_4	–	–
	W_5	–	0		W_5	–	–
	W_6	1.06	3		W_6	–	–
PB12-L(12–82)	W_1	19.19	3	PB12-R(100–170)	W_1	15.18	3
	W_2	21.14	2		W_2	3.26	3
	W_3	13.74	3		W_3	–	0
	W_4	11.20	3		W_4	–	0
	W_5	21.73	2		W_5	–	0
	W_6	36.86	2		W_6	8.97	2
PB12-L(124–169)	W_1	–	0	PB12-R(358–403)	W_1	–	–
	W_2	2.23	3	Uncorroded	W_2	–	–
	W_3	–	0		W_3	–	–
	W_4	–	0		W_4	–	–
	W_5	4.24	3		W_5	–	–
	W_6	23.96	3		W_6	–	–
PB13-L(1–46)	W_1	–	0	PB13-R(0–70)	W_1	3.11	3
	W_2	–	0		W_2	7.78	2
	W_3	–	0		W_3	6.58	2
	W_4	22.85	1		W_4	16.71	2
	W_5	7.78	3		W_5	22.03	2
	W_6	–	0		W_6	27.02	2
PB13-L(108–178)	W_1	34.38	3	PB13-R(70–115)	W_1	–	0
	W_2	–	0		W_2	20.23	3
	W_3	–	0		W_3	–	0
	W_4	–	0		W_4	–	0
	W_5	–	0		W_5	–	0
	W_6	–	0		W_6	–	0
PB14-L(10–55)	W_1	53.06	3	PB14-R(2–72)	W_1	18.19	2
	W_2	12.10	2		W_2	6.40	3
	W_3	17.60	2		W_3	7.98	3
	W_4	14.94	3		W_4	10.31	3
	W_5	17.89	2		W_5	9.86	2
	W_6	12.80	3		W_6	23.69	3
PB14-L(455–500)	W_1	–	–	PB14-R(77–122)	W_1	–	–
Uncorroded	W_2	–	–	(NEGLECTED)	W_2	–	–
	W_3	–	–		W_3	–	–
	W_4	–	–		W_4	–	–
	W_5	–	–		W_5	–	–
	W_6	–	–		W_6	–	–

** Where W stands for wire and the number ranging from 1 to 6 identifies the numbering of external wires.

References

[1] C. H. Jeon, C. D. Nguyen, and C. S. Shim, "Assessment of mechanical properties of corroded prestressing strands," *Appl. Sci.*, vol. 10, no. 12, 2020, doi: 10.3390/APP10124055.

[2] M. Di Prisco, Critical infrastructures in Italy: State of the art, case studies, rational approaches to select the intervention priorities, in: in *Proceedings of the fib Symposium 2019: Concrete - Innovations in Materials, Design and Structures*, 2019, pp. 49–58.

[3] N. Lu, Y. Ma, and Y. Liu, "Evaluating probabilistic traffic load effects on large bridges using long-term traffic monitoring data," *Sensors (Switzerland)*, vol. 19, no. 22, pp. 5056: 1–16, 2019, doi: 10.3390/s19225056.

[4] R.W. Floyd, J.S. Pei, J.P. Wright, Simple model for time-dependent bond transfer in pretensioned concrete using draw-in data, Eng. Struct. 160 (2018) 546–553, https://doi.org/10.1016/j.engstruct.2018.01.031.

[5] M. Elices, A. Valiente, L. Caballero, M. Iordachescu, J. Fullea, J. Sánchez-Montero, V. López-Serrano, Failure analysis of prestressed anchor bars, Eng. Fail. Anal. 24 (2012) 57–66, https://doi.org/10.1016/j.engfailanal.2012.03.007.

[6] J. Sanchez, J. Fullea, C. Andrade, Corrosion-induced brittle failure in reinforcing steel, Theor. Appl. Fract. Mech. 92 (July) (2017) 229–232, https://doi.org/10.1016/j.tafmec.2017.08.006.

[7] W.-P. Zhang, C.-K. Li, X.-L. Gu, Y.-H. Zeng, Variability in cross-sectional areas and tensile properties of corroded prestressing wires, Constr. Build. Mater. 228 (2019) 116830, https://doi.org/10.1016/j.conbuildmat.2019.116830.

[8] V. Val, E.R. Melchers, Reliability of deteriorating rc slab bridges, J. Struct. Eng. 123 (12) (1997) 1638–1644.
[9] D.V. Val, Deterioration of strength of RC beams due to corrosion and its influence on beam reliability, J. Struct. Eng. 133 (9) (2007) 1297–1306, https://doi.org/10.1061/(asce)0733-9445(2007)133:9(1297).
[10] C.H. Jeon, J. Bin Lee, S. Lon, C.S. Shim, Equivalent material model of corroded prestressing steel strand, J. Mater. Res. Technol. 8 (2) (2019) 2450–2460, https://doi.org/10.1016/j.jmrt.2019.02.010.
[11] M.S. Darmawan, M.G. Stewart, Effect of pitting corrosion on capacity of prestressing wires, Mag. Concr. Res. 59 (2) (2007) 131–139, https://doi.org/10.1680/macr.2007.59.2.131.
[12] F. Vecchi, L. Franceschini, F. Tondolo, B. Belletti, J. Sánchez Montero, P. Minetola, Corrosion morphology of prestressing steel strands in naturally corroded PC beams, Construction and Building Materials 296 (2021) 123720, https://doi.org/10.1016/j.conbuildmat.2021.123720.
[13] A. Zona, L. Ragni, and A. Dall'Asta, "Finite element formulation for geometric and material nonlinear analysis of beams prestressed with external slipping tendons," *Finite Elem. Anal. Des.*, vol. 44, no. 15, pp. 910–919, 2008, doi: 10.1016/j. finel.2008.06.005.
[14] L. Wang, T. Li, L. Dai, W. Chen, K. Huang, Corrosion morphology and mechanical behavior of corroded prestressing strands, J. Adv. Concr. Technol. 18 (10) (2020) 545–557, https://doi.org/10.3151/jact.18.545.
[15] Z.H. Lu, F. Li, Y.G. Zhao, An investigation of degradation of mechanical behaviour of prestressing strands subjected to chloride attacking, Int. Conf. Durab. Concr. Struct. ICDCS 2016 (2016) 57–65, https://doi.org/10.5703/1288284316111.
[16] "ASTM G1-03. Standard practice for preparing, cleaning, and evaluating corrosion test specimens.," 2017.
[17] J. Sanchez, J. Fullea, C. Andrade, Fracto-surface mobility mechanism in high-strength steel wires, Eng. Fract. Mech. 186 (2017) 410–422, https://doi.org/10.1016/j.engfracmech.2017.11.003.
[18] J. Sanchez, J. Fullea, C. Andrade, C. Alonso, Stress corrosion cracking mechanism of prestressing steels in bicarbonate solution, Corros. Sci. 49 (2007) 4069–4080, https://doi.org/10.1016/j.corsci.2007.05.025.
[19] J.A. Morales, J. Torres, N. Rebolledo, J. Sanchez, Experimental and statistical analysis of the corrosion in tendons in contact with water, Front. Mater. 6 (2019), https://doi.org/10.3389/fmats.2019.00167.
[20] B. Belletti, J. Rodríguez, C. Andrade, L. Franceschini, J. Sánchez Montero, F. Vecchi, Experimental tests on shear capacity of naturally corroded prestressed beams, Struct. Concr. 21 (5) (2020) 1777–1793, https://doi.org/10.1002/suco.202000205.
[21] F. Vecchi, B. Belletti, L. Franceschini, C. Andrade, J. Rodriguez, and S. J. Montero, "Flexural Tests on Prestressed Beams Exposed to Natural Chloride Action," 2021, December 0., pp. 205–212.
[22] J. Blaber, B. Adair, A. Antoniou, Ncorr: open-source 2D digital image correlation matlab software, Exp. Mech. 55 (6) (2015) 1105–1122, https://doi.org/10.1007/s11340-015-0009-1.
[23] H. Schreier, J.-J. Orteu, M.A. Sutton (Eds.), Image Correlation for Shape, Motion and Deformation Measurements, Springer US, Boston, MA, 2009.
[24] Y. Zhan, R. Zhao, Z.J. Ma, T. Xu, R. Song, Behavior of prestressed concrete-filled steel tube (CFST) beam, Eng. Struct. 122 (2016) 144–155, https://doi.org/10.1016/j.engstruct.2016.04.050.